117 (2023) 205071

Contents lists available at ScienceDirect

Gas Science and Engineering

journal homepage: www.journals.elsevier.com/gas-science-and-engineering

Probing into the interactions among operating variables in blue hydrogen production: A new approach *via* design of experiments (DoE)

Shervan Babamohammadi, William George Davies, Salman Masoudi Soltani *

Department of Chemical Engineering, Brunel University London, Uxbridge, UB8 3PH, UK

ARTICLE INFO

Keywords:
Steam methane reforming
Hydrogen
Carbon capture
Sorption enhanced

ABSTRACT

Anthropogenic CO_2 emission is a key driver in global warming and climate change. Worldwide, H_2 production accounts for 2.5% of this CO_2 emission. A shift to clean methods of hydrogen production is required to reduce CO_2 emissions, and to mitigate the effects of climate change. Developing optimised process models of H_2 production processes is required in order to investigate the effects of operational variables of the process and their impacts on key performance indicators (KPIs). Within this study, a detailed rate-based model was implemented to simulate the reformer in Sorption Enhanced Steam Methane Reforming (SE-SMR), as well as Sorption-Enhanced Auto-Thermal Reforming (SE-ATR) processes. The results indicate that the SE-ATR/ATR corresponds to a significantly improved performance over the SMR with the optimal operating conditions for achieving the desired KPIs, including hydrogen purity (86%), hydrogen yield (36%), methane conversion (99%), and carbon capture rate (50%) at a temperature of 720 °C, a pressure of 20 bara, and an S/C ratio of 6. Whereas with SMR, the temperature, pressure, and S/C ratio should be adjusted to 975 °C, 20 bara, and 6, respectively, to achieve a hydrogen purity of 84%, a hydrogen yield of 42%, a methane conversion of 96%, and a carbon capture rate of 48%. The study provides insights into the optimal operating conditions to achieve maximum efficiency in the reformer, and demonstrates the effectiveness of incorporating DoE within process modelling as a tool for optimisation.

1. Introduction

1.1. Research background

Over the last century, the Earth's surface temperature has increased by an average of 0.08 °C per decade globally, according to data spanning from 1880 to 1981. This has increased by more than two-fold between 1981 and 2012 (i.e. 0.18 °C every decade) (NOAA, 2022). The Intergovernmental Panel on Climate Change (IPCC) reported that by 2100, the average global temperature would be 1.4–4.4 °C higher than pre-industrial levels (IPCC, 2022). This would bring about severe complications for the global ecosystems e.g. sea-level rise, flooding, ocean acidification, loss of crops and significant loss of species (IPCC, 2022).

Climate change is a direct result of the increases in global anthropogenic greenhouse gas emissions (GHGs), amongst which CO_2 has been identified as the key contributor to the temperature increase (Babamohammadi et al., 2021). The 2021 annual emission rate of CO_2 from anthropogenic sources was 39.2 Giga tonnes (Crippa et al., 2022) with the majority of this coming from the energy sector, chemical industries, transportation and cement manufacturing respectively (Abbas et al., 2017c). Research indicates that by 2050, global energy consumption will have increased by about 50%, which could bring about both political and economic turmoil alike (El Hajj Chehade et al., 2020). The growing concerns over energy security, the continual depletion of fossil fuels, anthropogenic carbon dioxide emissions, and the resulting changing climate has incentivised research and development in novel directions to further secure energy demands more effectively, whilst ensuring it is done sustainably and in an ecologically friendly fashion.

As part of the pathway to clean energy and reducing CO_2 emissions, solar, wind and green hydrogen have been identified as key energy vectors to ensure a just transition. However, there are drawbacks such as the cost of scale-up, regional limitations and intermittency of these technologies means that the development of renewable energy technologies is needed to ensure that they are clean but also do not raise costs significantly (BEIS, 2022; IEA, 2021; IPCC, 2022). Hydrogen has been recognised to be an inseparable part of the transition into a green economy. The global hydrogen review issued by the international energy agency (IEA) IEA, 2021 reported that around 90 Mt of hydrogen were required globally in 2020, an increase of 50% since 2000 (IEA,

* Corresponding author.
E-mail address: Salman.MasoudiSoltani@brunel.ac.uk (S. Masoudi Soltani).

https://doi.org/10.1016/j.jgsce.2023.205071
Received 1 May 2023; Received in revised form 9 July 2023; Accepted 12 July 2023
Available online 14 July 2023

Nomenclature

ATR	Auto Thermal Reforming
BEIS	Department for Business, Energy and Industrial Strategy
CAPEX	Capital Expenditure
DoE	Design of Experiments
GFD	General Full Factorial Design
GLHHW	Generalised-Langmuir-Hinshelwood-Hougen-Watson
GHG	Greenhouse Gas Emissions
HTE	High-Temperature Electrolysis
IPCC	Intergovernmental Panel on Climate Change
IEA	International Energy Agency
KPIs	Key Performance Indicators
LHHW	Langmuir-Hinshelwood-Hougen-Watson
NOAA	National Oceanic and Atmospheric Administration
OFAT	One Factor at a Time
OPEX	Operational Expenditure
PSA	Pressure Swing Adsorption
SE-ATR	Sorption Enhanced Auto Thermal Reforming
SE-CLC	Sorption Enhanced Chemical Looping Combustion
SE-SMR	Sorption Enhanced Steam Methane Reforming
SMR	Steam Methane Reforming
WGS	Water Gas Shift

2021). This includes more than 70 Mt of pure hydrogen and about 20 Mt of hydrogen mixed with other fuel gases for industries like steel manufacturing and methanol production (IEA, 2021). Hydrogen is also essential in ammonia, oil refining and chemical production industries. Due to the absence of CO_2 as a combustion product in the flue gas, hydrogen can also play a key role in the decarbonisation of transport, residential, industrial, and power sectors.

Hydrogen is frequently referred to as the future fuel since it can be used to generate power with no GHG emissions. According to the IEA Global Hydrogen Review, in 2020, 6% of global natural gas demand (240 bcm) was utilised to meet 60% of hydrogen production worldwide (IEA, 2021). Although hydrogen combustion leads to zero GHG emission, the generation of hydrogen from fossil fuels (e.g. natural gas) was responsible for the simultaneous co-generation of over 900 Mt of direct CO_2 emissions in 2020 (i.e. 2.5% of the world's energy and industrial CO_2 emissions). In order to put this into perspective, this is comparable to the carbon emissions of Indonesia and the United Kingdom combined. Consequently, emissions from hydrogen production must be decreased for a clean energy transition (IEA, 2021).

Hydrogen can be produced *via* a number of processes, including high-temperature electrolysis (HTE), wind (or solar) water electrolysis, gasification, and steam methane reforming (SMR) (El Hajj Chehade et al., 2020; Mehmeti et al., 2018). Among these, steam methane reforming accounts for more than half of the global hydrogen production (El Hajj Chehade et al., 2020; Faheem et al., 2021; Masoudi Soltani et al., 2021). In a conventional SMR process, high-temperature compressed steam and methane are delivered to the reformer, where methane is reformed into hydrogen and carbon according to the reforming reaction (R 1). For this process to initiate and proceed, heat must be added to overcome the thermodynamic energy barrier (i.e. an endothermic reaction - $\Delta H_{298K} = 206$ kJ/mol). The produced syngas is next fed to the shift reactor, where the water-gas shift (WGS) reaction takes place (R 2). The inclusion of specific catalysts (i.e. Ni, Ir and Pt-based) benefits both processes by reducing the energy that is needed for this endothermic reaction. Furthermore, incorporating supports such as Al_2O_3 can be utilised to reduce the effects of poisoning and improve conversion efficiency (Masoudi Soltani et al., 2021). Commonly nickel is used within the industry due to the cost of Ir and Pt-based catalysts. Since the WGS reaction occurs as a side reaction to SMR, the overall reaction will be explained according to R 3:

$$CH_4 + H_2O \leftrightarrow CO + 3H_2 \Delta H_{298K} = 206\ kJ/mol \quad \text{R 1}$$

$$CO + H_2O \leftrightarrow CO_2 + H_2 \Delta H_{298K} = -41\ kJ/mol \quad \text{R 2}$$

$$CH_4 + 2H_2O \leftrightarrow CO_2 + 4H_2 \Delta H_{298K} = 164.9\ kJ/mol \quad \text{R 3}$$

The separation and purification procedures start once the methane and steam have (almost) entirely transformed into H_2 and CO_2. In a typical SMR, the CO_2 is often removed after the reformer, using an amine absorption unit, and the H_2 is further purified using pressure swing adsorption (PSA) to meet commercial product specifications. For example, the Hydrogen Purity report by Hy4Heat in BEIS recommends a minimum purity level of 98% for hydrogen for domestic applications (Brown et al., 2019). This purity is not achievable by SMR alone and requires further purification *via* PSA. However, reaching a purity close to 98% can optimise the operational and capital costs of subsequent PSA units.

The SMR and WGS reactions are restricted by thermodynamic limitation and chemical equilibrium, meaning that the complete conversions of methane and carbon monoxide are not achievable in one reactor (Shahid et al., 2021; Silva et al., 2017). Moreover, due to the highly endothermic reaction of methane reforming (R 1), the SMR process is very energy intensive with significant capital and operational expenses (Faheem et al., 2021).

One possible route to supply the reformer with energy is to burn a portion of methane with oxygen or auto-thermal reforming (ATR), according to the general combustion reaction:

$$CH_4 + 2O_2 \rightarrow CO_2 + 2H_2O \Delta H_{298K} = -802.7\ kJ/mol \quad \text{R 4}$$

The heat generated by the highly exothermic reaction (R 4) can (partly) drive the SMR reaction (R 1) and other utilities in the process. The ATR approach (i.e. methane combustion) also helps to improve the H_2 purity and increases the driving force profile of CO_2 removal (Faheem et al., 2021).

The other advancement which has been focused on over the past decade is the *in-situ* CO_2 separation by using high-temperature CO_2 sorbents such as CaO (Faheem et al., 2021; Masoudi Soltani et al., 2021). Such processes are referred to as sorption-enhanced steam methane reforming (SE-SMR). Removing CO_2 from the reforming equation (R 1) helps the forward reaction and produces more hydrogen (i.e. Le-Chatelier's principle) (Masoudi Soltani et al., 2021). In addition to increasing the reformer's productivity, *in-situ* CO_2 capture also creates a more compact process unit (*2-in-1*), which may optimise the process's capital expenditures (CAPEX). In addition, having less CO_2 in the outlet gas stream improves the H_2 purity (from 70% H_2 to 98% H_2) (Cherbański and Molga, 2018; Wang et al., 2021). This will reduce the steam demand of the process and enable more moderate operating conditions (from a temperature of 800–1000 °C to 450–490 °C) (Di Giuliano and Gallucci, 2018), which potentially favourably impacts the operational expenses (OPEX) (Faheem et al., 2021; Masoudi Soltani et al., 2021). Various research focusing on the SE-SMR process have employed CaO as a CO_2 sorbent in recent years (Abbas et al., 2017a, 2017b; 2017c; Faheem et al., 2021; Lee et al., 2004; Shahid et al., 2021). The reaction is explained *via* R 5:

$$CO_2 + CaO(s) \leftrightarrow CaCO_3(s) \Delta H_{298K} = -178.8\ kJ/mol \quad \text{R 5}$$

Integration of simultaneous methane combustion and CO_2 sorption in conventional steam methane reforming was not well studied until just recently. In 2021, Faheem et al. (2021) investigated auto-thermal reforming coupled with sorption-enhanced reforming (SE-ATR). Their

work demonstrated efficient H_2 generation, CO_2 capture and CH_4 conversion, suggesting high potential for industrial adoption. The results of their study have been the drive and rationale behind our current research, aiming to further the process integration in this realm of research.

1.2. Literature review

Currently, the latest research focuses on using a thermodynamic-based model such as equilibrium-based reactors and Gibbs free-energy models for both the reformer and water-gas shift reactor. Antzara et al. (2015) did a thermodynamic analysis to compare SMR, SE-CLC-SMR and SE-SMR, using Gibbs free energy reactor. Yan et al. (2020) compared six process configurations of SE-SMR using a Gibbs reactor as the module for the reactor for each process configuration, whilst Maqbool et al. (2021) modelled a 1-D heterogeneous catalytic SMR reforming over 12 different catalysts. They then used a similar model to compare SMR, SE-SMR and SE-ATR (Faheem et al., 2021). However, detailed exploitation of this process needs to utilise a kinetic-based reactor model to provide a clearer understanding of how the rate at which the reaction proceeds.

To scrutinise the key variables in the hydrogen production process, sensitivity analysis is a conventional method to reveal the impact of an independent factor on a dependent variable. The backbone of the sensitivity study is the one-factor-at-a-time (OFAT) method. In this approach, one factor is incrementally varied while keeping other independent factors constant, and the effect of this change is investigated on a set of key performance indicators (KPIs) – i.e. the independent variables (Babamohammadi et al., 2018). However, sensitivity analysis fails to reveal the presence of any interaction among several factors, and their impacts on the desired KPIs. This is especially important when considering a process model where many operational variables are involved since this analysis does not give a clear indication of how these operating variables interact.

Within the literature, as mentioned above the conventional method of optimisation of clean hydrogen production is a sensitivity analysis, often utilised within the literature to provide optimal operating conditions *via* the sequential changing of key operating parameters such as temperature, pressure, and S/C ratio. Whilst it is a useful method to understand the impact of individual parameters on KPIs, further advancement is needed within the optimisation of process models.

Design of Experiment (DoE) is a powerful tool, enabling us to probe into such interactions. The DoE, unlike the sensitivity analysis, investigates the interactions between the parameters and provides more information about the whole process (Gorbounov et al., 2022). Utilising DoE provides a more robust approach to optimisation by investigating the interaction of operating parameters. The parallel evaluation of a combination of input parameters in DoE methods can provide a greater understanding of the interaction of the parameters and identification of which variables are the key operating parameters, whilst simultaneously increasing the speed at which optimisation can occur.

The DoE has almost exclusively been used in experimental campaigns, such as the application of DoE within the optimisation of adsorbent synthesis for CO_2 capture (Gorbounov et al., 2023; Mozaffarian et al., 2019) as well as the optimisation of adsorption processes such as PSA and temperature swing adsorption (TSA) (Saberimoghaddam and Nozari, 2017). Although it has been mainly used in experimental works recent work has looked into the incorporation of DoE into SMR modelling as well with a recent study by (Quirino et al., 2022) focused on the optimisation of an industrial SMR using DoE. This work highlights the potential of utilising DoE in process modelling, which provides in-depth detail of the interaction of the operating variables and how they impact KPIs.

1.3. Paper motivation

To the best of our knowledge, despite a significant amount of research on the modelling of SMR reactors, no detailed study combining the aforementioned solutions and their impact on the process's performance has been documented as of today, specifically the optimisation and subsequent comparison of the SMR and ATR reactors. Furthermore, the employment of equilibrium-based and the Gibbs free-energy model to describe the behaviour of the reformer is unable to provide comprehensive insights into the process characteristics due to the simplistic assumptions associated with these models.

In this work, we present a developed kinetic model of the SMR process with carbon capture combined with a novel approach to optimisation within the modelling and simulation of a blue hydrogen production process. A one-dimensional heterogonous reactor has been modelled in Aspen Plus. A kinetic-based model was employed to define the SMR and WGS reactions with a Generalised-Langmuir-Hinshelwood-Hougen-Watson (GLHHW) reaction model. The models are defined based on the literature data (Abbas et al., 2017c; Faheem et al., 2021; Halabi et al., 2008; Shahid et al., 2021; Singh et al., 2014; Xu and Froment, 1989) and precisely reordered to fit with the Aspen Plus form of equations.

Furthermore, this work presents a state-of-the-art approach to optimisation within modelling *via* the integration of DoE for optimisation of these four KPIs (H_2 yield (wt.% of CH_4), H_2 purity, CH_4 conversion, and CO_2 capture rate). These KPIs are important because they provide a quantitative measure of the efficiency and effectiveness of the hydrogen production process. By monitoring and optimising these KPIs, operators can ensure that the process is operating efficiently, cost-effectively, and sustainably. In the following sections, a detailed methodology is outlined highlighting how the rate-based model was developed as well as the DoE that was employed within this study. The results section provides an in-depth analysis and discussion of the model description and interactions between the operating parameters with respect to each KPI before summarising the key results from this optimisation.

2. Methodology

2.1. Design of experiments

A Design of Experiment (DoE) (i.e. General Full Factorial Design (GFD)) with four independent variables was initially designed to inform the execution of the process model. In a full factorial design, all possible combinations of the levels of the factors are investigated. The factors are the independent variables or inputs that are believed to have an effect on the response variable, which is the dependent variable or response. Each factor is typically defined at two or more levels (Durakovic, 2018). The DoE allowed us to probe into the effects of interactions between the studied operating variables and the optimum operating envelopes for our pre-defined set of KPIs. Since in this case, three factors (Temperature, Pressure, and Steam/Methane) have more than two levels, the GFD can be used instead of a 2-level full factorial design to build all possible combinations of the desired levels. The performance of the individual process has been analysed in terms of the H_2 yield, H_2 purity, CH_4 conversion and CO_2 capture rate (i.e. KPIs) under various operating conditions of temperature (400–1000 °C), pressure (1–30 bara) and S/C (1–6), both with and without methane combustion unit (ATR zone). The temperature is set for the feed of the reformer and pressure is set for the whole process.

Two sets of 64 simulation runs under different conditions (with and without ATR) were designed. This led to a total number of 128 simulation runs, the data of which was next statistically processed. Table 1 summarises the independent variables and their corresponding levels/codes investigated in this work.

Building upon the statistical analysis, the significant variables and their impacts on the responses were identified, and then a *metamodel* (i.

Table 1
The independent variables and their levels/codes are studied in this work.

Level	Code	Temperature (°C)	Pressure (bara)	Steam/ CH_4 *(mol/ mol)*	CH_4 combustion unit (option)
Level 1	−1	400	1	1	With (Code = −1)
Level 2	−0.33	600	10	2.5	Without (Code = +1)
Level 3	+0.33	800	20	4	
Level 4	+1	1000	30	6	

e. a simple semi-empirical mathematical model of the simulation) was developed accordingly. This metamodel gave us more insight into how changing a variable would affect the responses/KPIs and allowed us to study the interactions between different factors. This is important because the effect of one factor on the KPIs may depend on the level of another factor. Furthermore, the model can help to predict the responses within the range of variables and to identify the variables' values which would be able to optimise responses.

The following equations have been employed to calculate the H_2 yield (wt.% of CH_4), H_2 purity, CH_4 conversion, and CO_2 capture from the produced data, where '*n*' denotes the relevant molar amounts achieved by simulation (Faheem et al., 2021):

$$H_2\ Yield_{(wt\%\ of\ CH_4)} = \frac{mole\ weight\ of\ H_2 \times n_{H_2\ out}}{mole\ weight\ of\ CH_4 \times n_{CH_4\ in}} \times 100 \quad \text{Eq. 1}$$

$$H_2\ Purity_{(\%)} = \frac{n_{H_2 out}}{n_{H_2\ out} + n_{CH_4\ out} + n_{CO\ out} + n_{CO_2\ out}} \times 100 \quad \text{Eq. 2}$$

$$CH_4\ Conversion_{(\%)} = \frac{n_{CH_4\ in} - n_{CH_4\ out}}{n_{CH_4\ in}} \times 100 \quad \text{Eq. 3}$$

$$CO_2\ Capture_{(\%)} = \frac{n_{CH_4\ in} - n_{CH_4\ out} - n_{CO\ out} - n_{CO_2\ out}}{n_{CH_4\ in}} \times 100 \quad \text{Eq. 4}$$

2.2. Process design

Aspen Plus® simulation software (Version 12.1) was employed to simulate the designed processes and gather stream data to estimate operating conditions' influence using kinetic rate-based calculations. Fig. 1 represents the process flow diagrams for clean hydrogen production including the option of having the ATR zone. The simulation was based on a number of assumptions in order to avoid the complexity of the model i.e. steady state operation with no temperature gradient in the reactor, ideal gas behaviour, zero pressure drop in process, no catalyst degradation, no sorption degradation and no side reaction or carbonation or adsorption other than the reactions described in the introduction section.

The inlet of the reformer has been selected between two modes through a selector module, either with an ATR zone or without it. When the methane is combusted (within the ATR zone), the selector transfers the flow from the combustion chamber (the ATR zone) and in the absence of methane combustion, the "selector" uses the bypasses stream over the ATR zone. The *in-situ* CO_2 adsorption with CaO is designed by coupling a pair of stoichiometric reactors and separators for adsorption and sorbent regeneration. The output of this unit is a stream rich in hydrogen and steam. Then, hydrogen is separated from the steam in the condenser unit and sent to storage. Table 2 provides a description of the connecting streams, feed streams, product streams, and blocks.

2.3. Kinetic models

The reforming reaction has been modelled in a plug-flow reactor using the rate-based Langmuir-Hinshelwood-Hougen-Watson (LHHW) kinetic model. The *rate of reaction* (mol.kg_{cat}^{-1}.s^{-1}) for the reforming reaction of methane with steam in the presence of Ni–Al_2O_3 catalyst can be described by LHHW kinetic model as follows (Abbas et al., 2017a, 2017b; 2017c; Faheem et al., 2021; Shahid et al., 2021):

$$R_1 = \frac{k_1}{P_{H_2}^{2.5}} \left(P_{CH_4} P_{H_2O} - \frac{P_{H_2}^3 P_{CO}}{K_I} \right) \left(\frac{1}{\Omega^2} \right) \quad \text{Eq. 5}$$

where k_1 and K_I are the rate, and equilibrium constants for the SMR, and Ω is the adsorption term which are described as follows:

$$k_1 = k\ exp\left(\frac{-E}{RT}\right) = 1.17 \times 10^{15}\ exp\left(\frac{-240100}{RT}\right) \quad \text{Eq. 6}$$

$$K_I = exp\left(\frac{-26830}{T} + 30.114\right) \quad \text{Eq. 7}$$

$$\Omega = 1 + K_{CO}P_{CO} + K_{H_2}P_{H_2} + K_{CH_4}P_{CH_4} + K_{H_2O}\frac{P_{H_2O}}{P_{H_2}} \quad \text{Eq. 8}$$

K_i s are the adsorption equilibrium constant of components '*i*', and P_i is

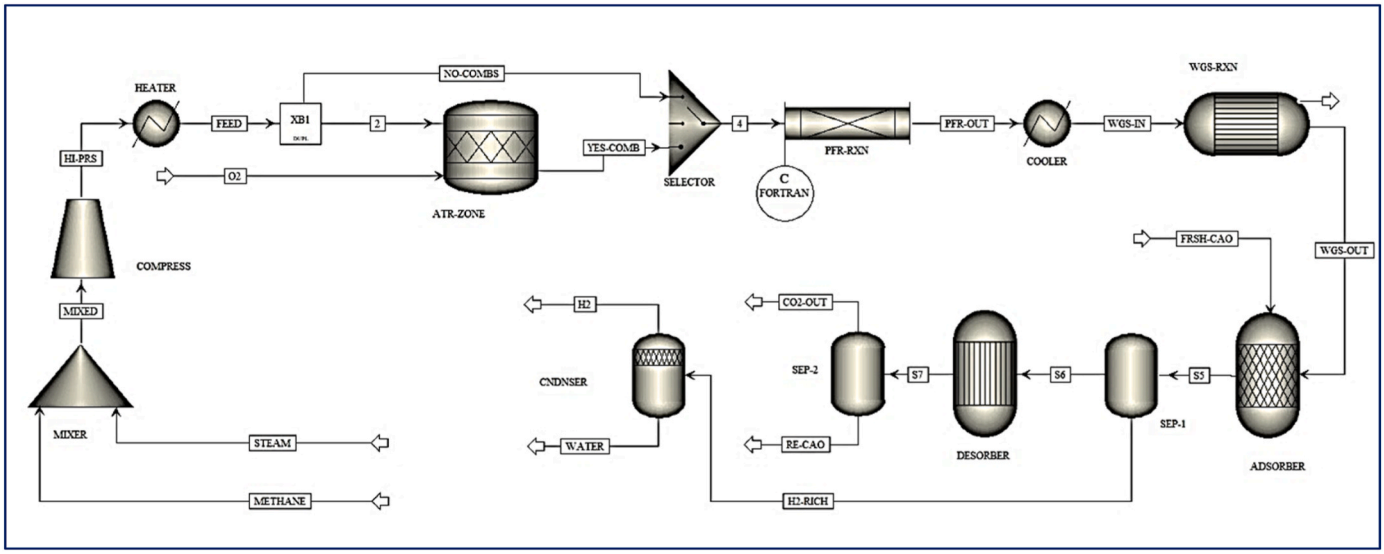

Fig. 1. The process flowsheet to model the clean hydrogen production in this work.

Table 2
Stream and Block's components summary for Fig. 1.

Stream/ Block	Component	Temperature	Pressure
Methane	CH_4 99.99% H_2 0.01% 1000 kmol/h	300 °C	1 bara
Steam	H_2O 100% (1–6) × 1000 kmol/h	300 °C	1 bara
Compress	Compressor (Isentropic 72%)	Inlet stream temperature	1-30 bara
Heater	Heater	400–1000 °C	Inlet stream pressure
PFR-RXN	PFR Reactor	Inlet stream temperature	Inlet stream pressure
Cooler	Heater	ΔT = −150 °C	Inlet stream pressure
WGS-RXN	REquil Reactor	Inlet stream temperature	Inlet stream pressure
O2	O_2 300 kmol/h	25 °C	Inlet stream pressure
ATR-zone	RStoic model	Inlet stream temperature	Inlet stream pressure
Frsh-CaO	CaO 100%	25 °C	Inlet stream pressure
Adsorber	RStoic model	Inlet stream temperature	Inlet stream pressure
SEP-1	Flash2 separator	Inlet stream temperature	Inlet stream pressure
Desorber	RStoic model	Inlet stream temperature	Inlet stream pressure
SEP-2	Flash2 separator	Inlet stream temperature	Inlet stream pressure
CNDNSER	Flash2 separator	50 °C	Inlet stream pressure

the partial pressure of that component. The adsorption term uses Van't Hoff parameters, as listed in Table 3 (Singh et al., 2014).

A WGS reactor was used to construct a more realistic simulation that replicates the circumstances of an actual process. The WGS reactor converts the remaining carbon monoxide exiting from the reformer to hydrogen to increase the yield of hydrogen according to Eq. (2). Similar to the reforming reaction, the WGS reaction also follows the LHHW model as follows:

$$R_2 = \frac{k_2}{P_{H_2}}\left(P_{CO}P_{H_2O} - \frac{P_{H_2}P_{CO}}{K_{II}}\right)\left(\frac{1}{\Omega^2}\right) \quad \text{Eq. 9}$$

k_2 and K_{II} are the rate and equilibrium constant for WGS reaction:

$$k_2 = k\ exp\left(\frac{-E}{RT}\right) = 5.43 \times 10^5\ exp\left(\frac{-67130}{RT}\right) \quad \text{Eq. 10}$$

$$K_{II} = exp\left(\frac{4400}{T} - 4.036\right) \quad \text{Eq. 11}$$

The rate of the overall SMR reaction (R 3) is, therefore, described as:

$$R_3 = \frac{k_3}{P_{H_2}^{3.5}}\left(P_{CH_4}P_{H_2O}^2 - \frac{P_{H_2}^4 P_{CO}}{K_{III}}\right)\left(\frac{1}{\Omega^2}\right) \quad \text{Eq. 12}$$

k_3 and K_{III} are the rate and equilibrium constant for the overall reaction:

Table 3
The Van 't Hoff parameters used in the GLHHW correlation.

Equilibrium constant	Pre-exponential factor	Units	E_a (kJ/mol)
K_{CH4}	6.65E-04	atm^{-1}	−38.28
K_{H2O}	1.77 E+05	-	−88.68
K_{H2}	6.12E-09	atm^{-1}	−82.9
K_{CO}	8.23E-05	atm^{-1}	−70.65

$$k_3 = k\ exp\left(\frac{-E}{RT}\right) = 2.83 \times 10^{14}\ exp\left(\frac{-243900}{RT}\right) \quad \text{Eq. 13}$$

$$K_{III} = K_I \times K_{II} \quad \text{Eq. 14}$$

Aspen Plus, however, does not directly support the rate expression detailed above. Indeed, the following equations are the general equation for LHHW in Aspen Plus:

$$R = \frac{(kinetic\ factor) \times (driving\ force)}{(adsorption\ term)} \quad \text{Eq. 15}$$

where,

$$kinetic\ factor = k\left(\frac{T}{T_o}\right)^n e^{-\left(\frac{E}{R}\right)\left(\frac{1}{T}-\frac{1}{T_o}\right)} \quad \text{Eq. 16}$$

$$driving\ force = K_1\prod_{i=1}^{N} C_i^{\alpha} - K_2\prod_{i=1}^{N} C_i^{\beta} \quad \text{Eq. 17}$$

$$adsorption\ term = \left[\sum_{i=1}^{M} K_1\left(\prod_{J=1}^{N} C_J^M\right)\right]^m \quad \text{Eq. 18}$$

$$K = A\ \exp\left(\frac{B}{T}\right)T^C\ \exp\ (DT) \quad \text{Eq. 19}$$

Therefore, it is necessary to rearrange equations Eq. 5-14 in order to identify the corresponding model's coefficients and parameters. The Aspen parameters for each reaction are tabulated in Table 4.

The thermodynamic fluid package of Peng-Robinson is used for the simulation as this model is suitable for light gases (i.e. hydrogen, oxygen, carbon monoxide, carbon dioxide, and methane) in the combination of non-polar or slightly polar compounds (Al-Malah, 2016; El Hajj Chehade et al., 2020). Steam and methane are the feedstock in the process with an initial temperature and pressure of 300 °C and 1 bara. Both streams are mixed in the mixer, then compressed isentropically to 5 bara (with an efficiency of 72%) and without any intercooler due to the relatively low-pressure increase, and then heated up to the desired temperature based on Table 1. A very small amount of hydrogen (i.e. 0.01 kmol/h or 0.001%) is added to the feed stream to avoid division by zero in Eq. (5), Eq. (8), Eq. (9) and Eq. (12) (which would lead to the divergence of the model). The plug flow reactor is set to operate isothermally with a length of 10 m and a diameter of 0.2 m. The corresponding reactions in this reactor are described in Eqs. (1)–(3). The overhead discharge stream of the reformer is then fed into an equilibrium WGS reactor to enhance further CO conversion. The WGS reactor's discharge stream is then fed to the adsorber-desorber section to remove CO_2 and then separate hydrogen from the water.

Table 4
Aspen Plus parameters for GLHHW.

Parameters of GLHHW	k_i	n	E	A	B
***kinetic factor for R*$_1$**	1	0	0	–	–
***Forward reaction for R*$_1$**	–	–	–	34.69	−28877.9
***Reserve reaction for R*$_1$**	–	–	–	4.5845	−2049.07
***kinetic factor for R*$_2$**	1	0	0	–	–
***Forward reaction for R*$_2$**	–	–	–	13.20	−8074.18
***Reserve reaction for R*$_2$**	–	–	–	17.24	−12474.2
***kinetic factor for R*$_3$**	1	0	0	–	–
***Forward reaction for R*$_3$**	–	–	–	32.27	−29335.53
***Reserve reaction for R*$_3$**	–	–	–	7.20	−6905.53
K_{CO}	–	–	–	−9.4051	8497
K_{H_2}	–	–	–	−18.9117	9971
K_{CH_4}	–	–	–	−7.3157	4604
K_{H_2O}	–	–	–	12.084	−10666

3. Results and discussions

3.1. Model validation

The experimental study for steam methane reforming by Singh et al. (2014) was used to validate the modelling results in this work. A simulation run under the same operating conditions has been performed for this purpose, and the fractional CH_4 conversion result was compared with Singh's experimental data in Fig. 2. It is seen that methane conversion in the plug flow reactors (model vs experimental) increased quickly during the first metre of reactor's length and then began to level off. The mean error was calculated to be 3.19% (average mean error for 10 data points, $\varepsilon = \frac{\sum_1^n |\Delta x_i|/x_{Ei}}{n} \times 100, n = number\ of\ data\ points, \Delta x_i = difference\ between\ model\ and\ experiment$), indicating a good degree of accuracy of our developed model.

3.2. Model description and inter-parameter interaction

Several software options are available for GFD. In this study, the Design-Expert software (version 7.0) was used to accomplish the metamodel, explore interaction effects, and determine the optimal operating conditions. The simulation runs from the kinetic-based process model were initially subjected to regression analysis. During this stage, various mathematical models were evaluated, and their determination coefficients and associated *p*-values were determined. Among the available models in Design-Expert, for all 4 KPIs, the cubic-quadratic models were suggested by the software based on the combination of *F*-value and *p*-value. Each term of the model was carefully analysed, and those with high *p*-values were eliminated. Finally, through ANOVA, the following semi-empirical expressions were derived to model the KPIs:

$$H_2\ Yield = +29.88 + 13.09 \times A - 4.07 \times B + 4.45 \times C - 4.72 \times D + 0.41 \times A \times B + 1.85 \times A \times C + 9.70 \times A \times D - 0.21 \times B \times C - 1.80 \times B \times D + 1.24 \times C \times D - 2.68 \times A^2 + 1.19 \times B^2 - 2.37 \times C^2 + 1.39 \times A \times B \times C - 0.67 \times A \times B \times D + 0.76 \times A \times C \times D + 0.74 \times B \times C \times D + 2.88 \times A^2 \times B - 2.48 \times A^2 \times C - 1.62 \times A^2 \times D + 1.12 \times B^2 \times D - 1.03 \times C^2 \times D - 3.44 \times A^3 \quad \text{Eq. 20}$$

$$H_2\ Purity = +76.02 + 13.59 \times A - 4.52 \times B + 8.70 \times C - 3.55 \times D + 2.17 \times A \times B + 0.44 \times A \times C + 18.11 \times A \times D - 2.91 \times B \times D + 0.71 \times C \times D - 13.50 \times A^2 + 1.78 \times B^2 - 3.35 \times C^2 + 1.60 \times A \times B \times D + 1.13 \times A \times C \times D + 2.73 \times A^2 \times B - 3.30 \times A^2 \times C - 13.16 \times A^2 \times D - 1.49 \times A \times B^2 + 1.55 \times B^2 \times D - 1.70 \times C^2 \times D + 4.10 \times A^3 \quad \text{Eq. 21}$$

$$CH_4\ Conversion = +77.87 + 33.87 \times A - 9.78 \times B + 5.32 \times C - 23.56 \times D + 0.54 \times A \times B + 3.84 \times A \times C + 22.52 \times A \times D - 0.050 \times B \times C - 4.31 \times B \times D + 4.83 \times C \times D - 4.16 \times A^2 + 2.90 \times B^2 - 4.55 \times C^2 + 3.50 \times A \times B \times C - 2.11 \times A \times B \times D + 2.24 \times B \times C \times D + 6.83 \times A^2 \times B - 5.66 \times A^2 \times C + 2.70 \times B^2 \times D - 2.58 \times C^2 \times D - 9.15 \times A^3 \quad \text{Eq. 22}$$

$$CO_2\ Capture = +34.19 + 2.58 \times A - 2.99 \times B + 19.26 \times C + 1.44 \times D + 1.57 \times A \times B + 3.15 \times A \times C + 9.62 \times A \times D - 1.52 \times B \times C - 1.33 \times B \times D - 4.57 \times C \times D - 8.72 \times A^2 - 5.13 \times C2 + 1.00 \times A \times B \times D + 7.60 \times A \times C \times D + 2.38 \times A^2 \times B - 2.74 \times A^2 \times C - 9.32 \times A^2 \times D \quad \text{Eq. 23}$$

where *A*, *B*, *C* and *D* are the coded values of the temperature, the pressure, the S/C ratio, and the utilisation of ATR in the process, respectively as mentioned in Table 1.

Mainly three factors were considered to assess the reliability of the models: *F*-value, *p*-value and adjusted R-squared value (Amini et al., 2023). The *p*-values associated with all the expressions for the KPIs were found to be sufficiently low ($p - values \ll 0.05$), indicating their significance. Furthermore, the *F*-values for H_2 purity, H_2 Yield, CH_4 conversion, and CO_2 capture rate were determined to be 405.29, 160.79, 258.83, and 205.81, respectively. These values demonstrate that the models accurately represent the simulation data and effectively capture the influence of parameters on the responses. Additionally, the adjusted R-squared values for H_2 purity, H_2 Yield, CH_4 conversion, and CO_2 capture rate are 0.9853, 0.9666, 0.9771, and 0.9648, respectively. This further confirms that the simulation results align well with the provided semi-empirical expressions.

The identification and analysis of the inter-parameters interaction based on our pre-defined KPIs (CH_4 conversion, H_2 purity, H_2 yield (*wt. % of CH_4*), and CO_2 capture rate) are discussed in this section. Each simulation run was carried out according to the DoE design matrix to enable the study of the interaction of operational variables on the KPIs. The degree of parallelism between the graphs in the diagram is a primary indication of the severity of interactions between two parameters (i.e. S/C ratio, temperature and pressure). If the graphs' trends are parallel to some extent, then there is not much interaction between the parameters and vice versa; If graphs are not parallel at any range of variables, then in that range there is an interaction between the parameters.

3.2.1. CH_4 conversion

The interaction effects of temperature and pressure at the constant average S/C ratio (S/C = 4) on the CH_4 conversion are illustrated in Figs. 3 and 4 for the case in the absence of ATR and the case in the presence of ATR, respectively. The S/C ratio of 4 was chosen as it is the optimum S/C ratio reported elsewhere (Masoudi Soltani et al., 2021). In the first case (no ATR), the methane conversion increases with an increase in temperature. This trend can be attributed to the nature of the endothermic reforming reaction that favours the forward reaction. Overall, the conversion is higher at lower pressures. This is due to the fact that the number of product moles in the reforming reaction (R 3) is larger than the moles of the reactants, and therefore, according to Le

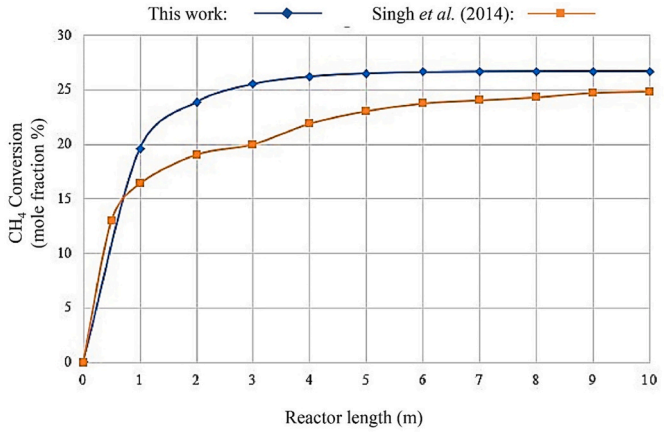

Fig. 2. The comparison of CH_4 fractional conversion from the Singh et al. experimental work and from the simulation of this work.

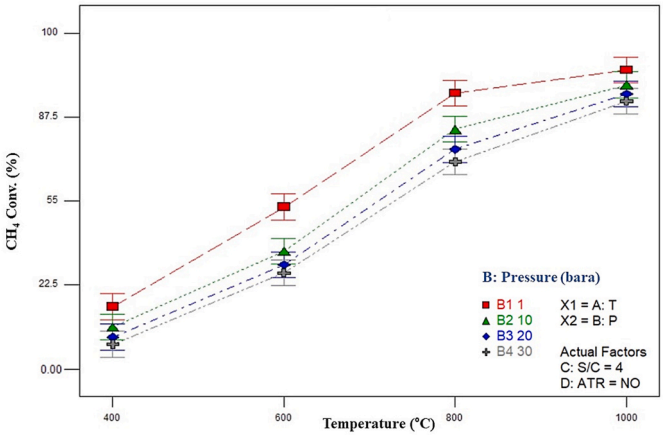

Fig. 3. Effect of temperature on CH_4 conversion for a fixed S/C of 4, and at different pressures and in absence of ATR.

Chatelier's principle (Masoudi Soltani et al., 2021), the reaction shifts to the reverse direction at high pressures, leading to a drop in CH_4 conversion.

As seen in Fig. 3, despite temperature and pressure affecting the methane conversion, they do not show significant interaction since the lines are almost parallel to each other. It means that the effect of temperature on methane conversion does not depend on the level of the pressure. In other words, the impact of temperature on methane conversion is consistent across all levels of pressure. There is a minor interaction which can be observed when the temperature approaches 1000 °C where the effect of pressure is slightly declined.

On the other hand, when ATR is utilised, temperature and pressure show an interaction on methane conversion (Fig. 4). At low pressures of 1 bara, the effect of temperature on methane conversion is not linear and first it increases the conversion rate and then after reaching 100% conversion at 600 °C it will remain the same till 800 °C and then falls to about 90%. At higher pressures, the conversion is generally lowered within the temperature range. The impact of pressure on methane conversion is not consistent across all levels of temperature, which indicate the presence of an interaction between temperature and pressure.

Therefore, the addition of the ATR leads to a significant interaction between temperature and pressure on methane conversion. It also increases the conversion across all pressures and temperatures studied in this work, which is the result of the activation of the combustion reaction (R 4) that reacts methane with oxygen.

By comparing Figs. 3 and 4 it shows that in the case of utilising ATR, the methane conversion can be 100% at 600 °C while in the absence of ATR, this would be about 95% at 1000 °C that indicate using ATR significantly increases the methane conversion even at lower temperatures.

Figs. 5 and 6 depict the interaction of temperature and S/C ratio on the methane conversion at the constant pressure of 20 bara, in the absence and presence of ATR respectively. The pressure of 20 bara is chosen here because, in industry, high-pressure H_2 is often desired downstream to the plant due to storage constraints. Therefore, it is not desirable to produce H_2 at low pressure and then employ high-pressure compressors to fulfil the downstream pressure specifications (Meyer et al., 2011). As we can see in Fig. 5, increasing the S/C ratio results in a higher conversion of methane because more steam can react with the methane to form hydrogen and carbon monoxide. Similarly, increasing the temperature also increases the conversion rate by providing more energy for the reaction. However, these two parameters have no interaction with each other on methane conversion.

However, by utilising ATR the presence of interaction can be observed (Fig. 6). The trend of methane conversion at S/C = 1 is completely different from the other S/C ratios. For example, from 400 to 800 °C the conversion of methane decreases when S/C = 1, whilst it increases when S/C = 6. This is because when ATR is utilised the highly exothermic reaction releases a significant amount of energy within the reformer and as a result the reforming reaction receives enough energy to be carried out and therefore the methane conversion increases anyhow. This implies that when ATR is utilised, the effects of the S/C ratio and temperature on methane conversion rate are dependent on each other and should be optimised together to achieve maximum conversion efficiency. This is the opposite of the case when ATR was not utilised, meaning that S/C and temperature are independent of each other and can be optimised separately to achieve maximum conversion.

3.2.2. H_2 yield

Figs. 7-12 show the effect of temperature, pressure, and S/C ratio on the hydrogen yield. As seen in Figs. 7 and 8, the effect of pressure and temperature on the H_2 yield is similar to their effect on methane conversion. On the other hand, the yield of H_2 is directly related to methane conversion. However, when the interaction effect of pressure and S/C ratio is scrutinised in Fig. 9 and Fig. 10, it can be concluded that the S/C and pressure have no interaction in both scenarios: with and without ATR. Both graphs are at a constant temperature of 800 °C which is around the conventional reforming temperature (Masoudi Soltani et al., 2021). According to the graph, increasing the pressure slightly decreases the hydrogen yield as expected based on Le Chatelier's principle. The effect is more dominant in the absence of ATR. Moreover, an S/C = 1 significantly decreases the hydrogen yield for both scenarios. Increasing

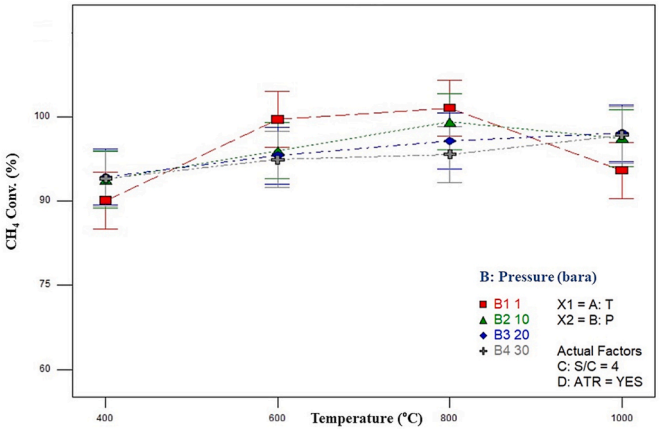

Fig. 4. Effect of temperature on CH4 conversion for a fixed S/C of 4, and at different pressures in the presence of ATR.

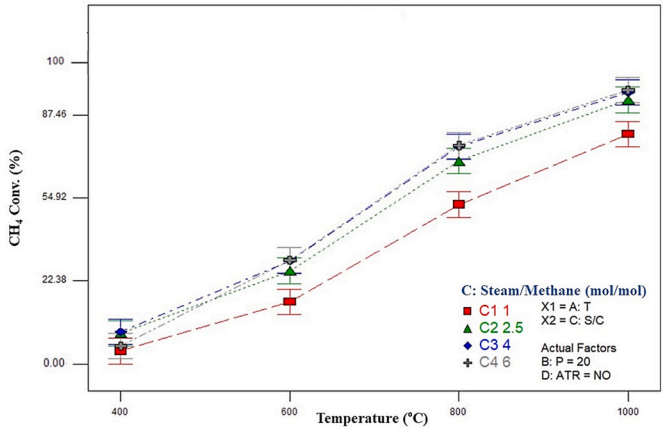

Fig. 5. Effect of temperature on CH_4 conversion at the fixed pressure of 20 bara and at different S/C ratios in the absence of ATR.

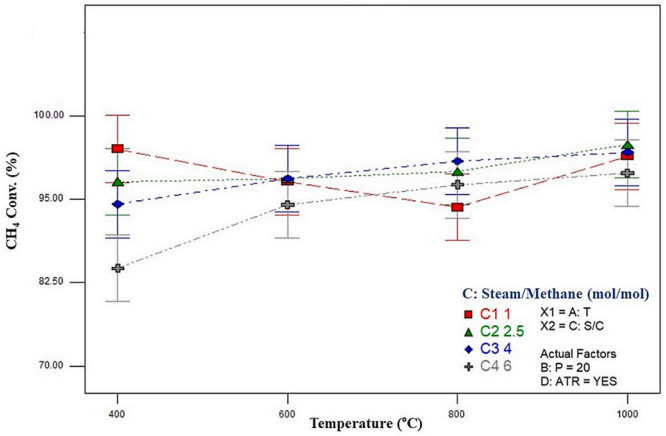

Fig. 6. Effect of temperature on CH_4 conversion at the fixed pressure of 20 bara and at different S/C ratios in the presence of ATR.

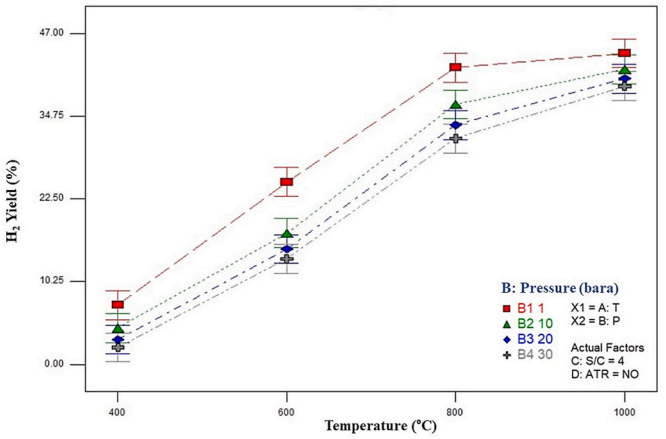

Fig. 7. Effect of temperature on H_2 yield for fixed S/C at 4 and at different pressure in the absence of ATR.

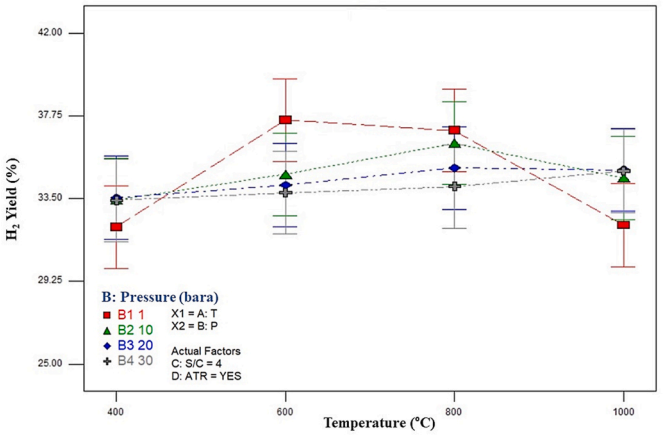

Fig. 8. Effect of temperature on H_2 yield for fixed S/C at 4 and at different pressure in the presence of ATR.

the S/C ratio together with decreasing pressure, amplifies the hydrogen yield. However, as mentioned earlier, low pressure is not desirable for the downstream, therefore, a pressure between 10 and 20 bara and S/C around 4–6 could be an optimised option for both scenarios. In the absence of ATR, it is essential that when using a high-pressure process

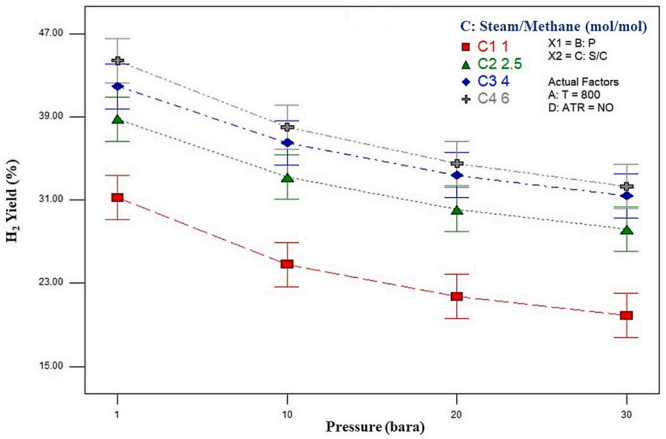

Fig. 9. Effect of pressure on H_2 yield at the fixed temperature of 800 °C and at different S/C ratios in the absence of ATR.

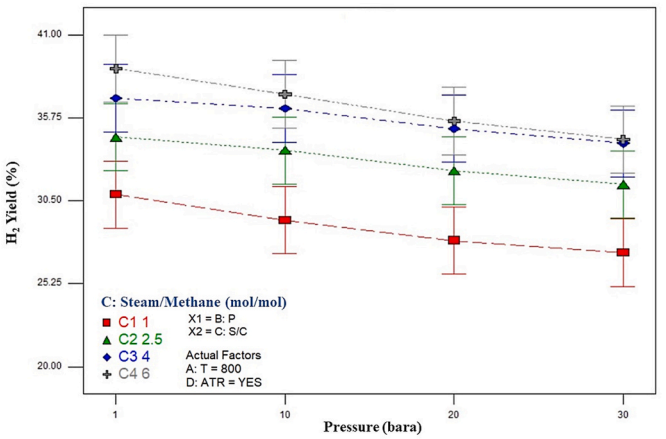

Fig. 10. Effect of pressure on H_2 yield at the fixed temperature of 700 °C and at different S/C ratios in the presence of ATR.

due to hydrogen storage limitations, employ elevated temperature as well to compensate for the negative effect of pressure. According to the model optimised by DoE, the highest hydrogen yield (=43.33%) can be achieved when the temperature is 1000 °C, the pressure is 10 bara, and the S/C ratio is 6 without using the ATR. If we want to utilise the ATR, then we can use 800 °C for temperature and other parameters remain the

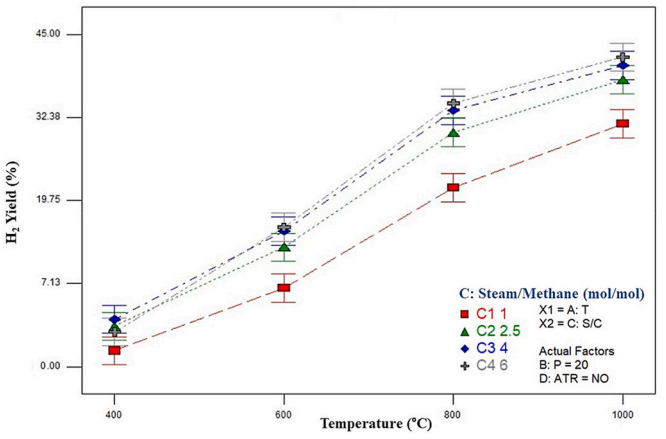

Fig. 11. Effect of temperature on H_2 yield at the fixed pressure of 20 bara and at different S/C ratios in the absence of ATR.

same, but the yield will be 37.22%.

Fig. 11 illustrates that there is not much interaction between temperature and S/C ratio, but only a minor one at the low-temperature zone (≈400–600 °C). Since the changes are not significant and the yield is low, we can neglect the interaction within that temperature zone. The observation is different when the ATR is utilised. As we see in Fig. 12, there is a clear interaction between temperature and S/C ratio, especially in low-temperature zone, or when S/C is equal to 1. This implies that in the presence of ATR, the relationship between the hydrogen yield, temperature and S/C ratio is not additive, but rather there is a non-additive effect. We can have a good hydrogen yield at the lowest temperature of 400 °C and an S/C ratio of 4 where if we increase the S/C ratio to 6, the yield significantly decreases. A good hydrogen yield at S/C = 6 can be achieved at higher temperatures (>600 °C).

3.2.3. H_2 purity

One of the essential KPIs in hydrogen production is the purity of the product. Due to high H_2 purity (>98%) requirements for end-use applications such as electronics, fuel cells, and polysilicon production, in most cases, a hydrogen purification unit such as membrane separation or PSA must be installed downstream to the production plant (Yan et al., 2020). The design and type of this unit depend on the purity of introduced hydrogen at the inlet stream, which consequently affects the process's CAPEX and OPEX. The effects of operational parameters on hydrogen purity are illustrated in Figs. 13-18.

Similar to methane conversion and hydrogen yield, when ATR is not utilised, graphs in Fig. 13 reveal that while temperature and pressure do have an impact on hydrogen purity individually, there is not a significant interaction between the two variables. This can be inferred from the parallel graphs, which suggest that changes in pressure do not affect the relationship between temperature and hydrogen purity. Specifically, the effect of temperature on hydrogen purity is consistent across all levels of pressure. Only a slight interaction is observed when the temperature approaches 1000 °C, where the effect of pressure slightly declines. This phenomenon is primarily due to the interplay between the thermodynamics and kinetics of the reforming reactions. When the temperature is near 1000 °C, the thermodynamic driving force for the reverse WGS reaction (R 2) to produce carbon monoxide from hydrogen is relatively high. This is while at higher temperatures in SMR, the reaction rates are faster and become more favourable in terms of their equilibrium compositions. This means that the concentrations of hydrogen and carbon monoxide tend to increase with increasing temperature. Therefore, at elevated temperatures, the effect of other parameters such as pressure on the final hydrogen composition will be insignificant.

By using the ATR in the process, the interaction between pressure and temperature is noticeable (Fig. 14). We can see the highest purity

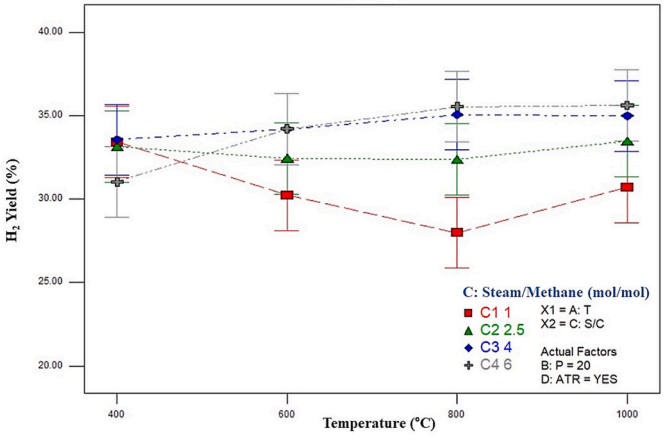

Fig. 12. Effect of temperature on H_2 yield at the fixed pressure of 20 bara and at different S/C ratios in the presence of ATR.

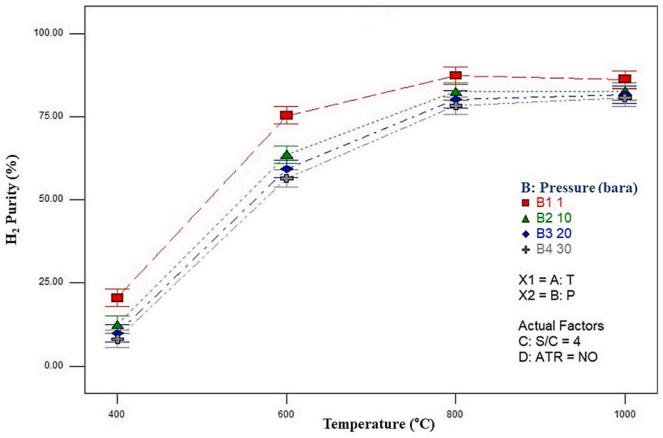

Fig. 13. Effect of temperature on H_2 purity for fixed S/C at 4 and at different pressure in the absence of ATR.

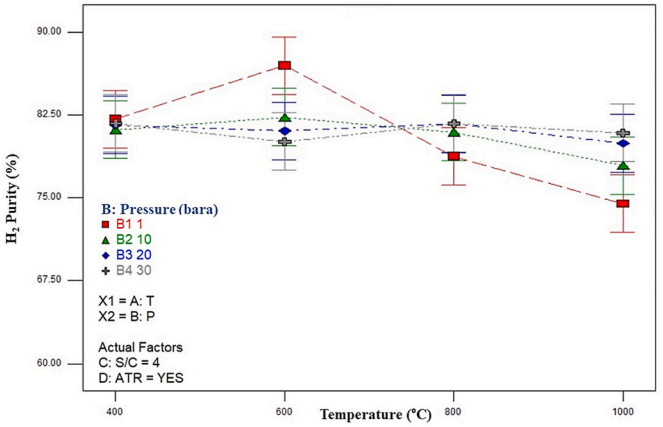

Fig. 14. Effect of temperature on H_2 purity for fixed S/C at 4 and at different pressure in the presence of ATR.

can be achieved at P = 1 bara and T = 600 °C. However, this pressure is not desirable as mentioned earlier. Therefore, if we increase the pressure to 10–20 bara, we need to increase the temperature to 800 °C as well to achieve an acceptable purity. We can also observe that when ATR is utilised, the dependency of KPIs (methane conversion, hydrogen yield and hydrogen purity) on temperature is almost diminished. It is mainly because ATR provides needed energy for the reaction in the reformer to carry out, therefore the gas inlet temperature is not affecting the KPIs significantly anymore.

From Fig. 15 and Fig. 16, we can see that there is no interaction between pressure and S/C ratio on hydrogen purity. In fact, pressure and S/C both have significant effects on the purity of hydrogen independently. Increasing the pressure in the reformer can indeed lead to a decrease in hydrogen purity. This is because higher pressures favour the reverse reaction, which reduces the concentration of hydrogen by converting it into carbon monoxide, thus reducing the hydrogen purity. On the other hand, the S/C ratio also affects hydrogen purity. The S/C ratio determines the availability of steam for the reforming reaction. Higher S/C ratios provide more steam, which helps in promoting the reforming reaction and increasing the hydrogen yield, consequently increasing the hydrogen purity. This trend is regardless of changes in the pressure. However, when ATR is used, the influence of pressure is different. In the presence of ATR, increasing the pressure slightly increases the hydrogen purity. This is the opposite when ATR is not utilised in the process. With the utilisation of ATR, a combination of oxidation and steam reforming reactions takes place simultaneously, which can lead to different

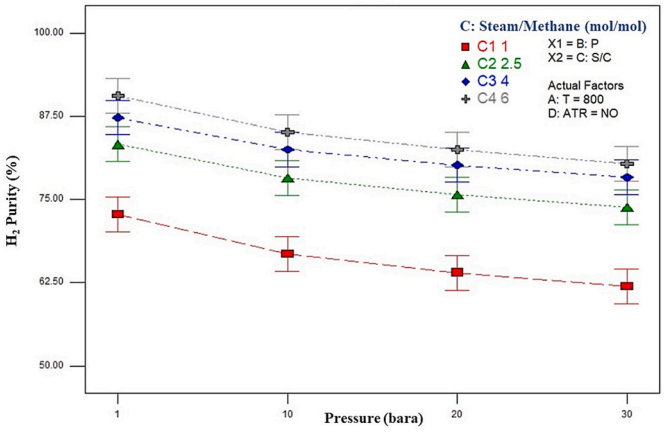

Fig. 15. Effect of pressure on H_2 purity at the fixed temperature of 800 °C and different S/C ratios in absence of ATR.

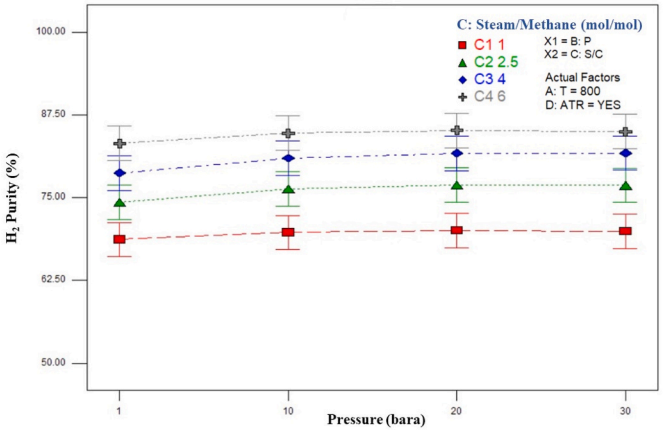

Fig. 16. Effect of pressure on H_2 purity at the fixed temperature of 800 °C and different S/C ratios in the presence of ATR.

behaviour compared to conventional SMR. The simultaneous combustion in ATR provides additional heat, which can compensate for any decrease in reaction rates caused by higher pressure. This helps to maintain the reaction kinetics and minimise the effects of pressure on the overall process, resulting in a reduced dependency of hydrogen purity on pressure.

Fig. 17 depicts the influence of temperature and S/C ratio on

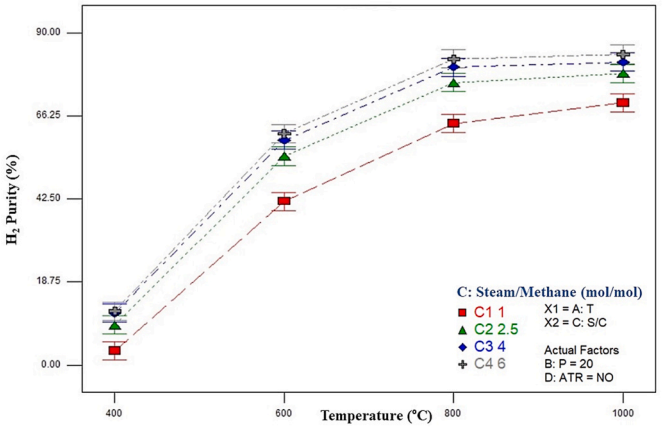

Fig. 17. Effect of temperature on H_2 purity at the fixed pressure at 20 bara and different S/C ratios in the absence of ATR.

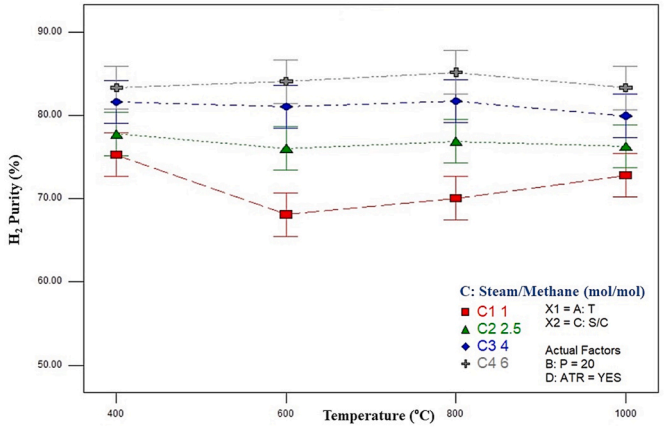

Fig. 18. Effect of temperature on H_2 purity at the fixed pressure at 20 bara and different S/C ratios in the presence of ATR.

hydrogen purity in the absence of ATR and it repeats the same trend for the other two KPIs discussed (methane conversion and hydrogen yield). The increase in temperature promotes the forward reaction and enhances the equilibrium shift towards the formation of hydrogen. Additionally, higher temperatures help overcome the activation energy barrier, facilitating the reaction kinetics and increasing the reaction rate. Regardless of the level of S/C, the purity of hydrogen is increased by temperature. With higher S/C ratios, there is a greater supply of steam, which promotes the reforming reaction and can enhance the conversion of methane into hydrogen. Consequently, the S/C ratio, together with temperature, affects the hydrogen purity in the system.

Fig. 18 also indicates that there is no significant interaction between the temperature and S/C ratio for the process with ATR as well. The hydrogen purity increased by increasing the S/C ratio, however, with increasing the temperature the purity is not changing significantly because the combustion heat produced by ATR has already provided enough energy for endothermic reforming reaction to produce the maximum hydrogen. Only at a low S/C ratio (S/C = 1), a slightly different trend is observed for hydrogen purity versus temperature which is due to the lack of enough steam to react with methane. Utilising the ATR can result in higher hydrogen purity within the temperature range because it leads to producing more steam and consuming methane according to (R 4) and consequently increases hydrogen purity.

Based on the DoE optimised model, the highest hydrogen purity (=85.60%) can be achieved when the temperature is 600 °C, the pressure is 10 bara, and the S/C ratio is 6 in the presence of the ATR. If we do not want to use the ATR, then based on the model, the temperature, pressure, and S/C ratio should be 1000 °C, 10 bara and 6. At this condition, the hydrogen purity will be 85.20%.

3.2.4. CO_2 capture rate

Figs. 19 and 20 provide insights into the effect of temperature, pressure, and ATR on the CO_2 capture rate by CaO. In the absence of ATR (Fig. 19), the CO_2 capture rate increases with temperature from 400 to 800 °C, regardless of the pressure level. This is because the optimal operating temperature for carbonation is about 700 °C to compromise higher conversion in an exothermic reaction (R 5) (Rodriguez et al., 2008). However, beyond 800 °C, the CO_2 capture rate decreases, possibly due to the thermal decomposition of $CaCO_3$ formed during the reaction, which forms CO_2 and CaO and consequently reduces the capture rate. Moreover, the lack of interaction between temperature and pressure on the CO_2 capture rate in Fig. 19 suggests that pressure has little effect on the reaction kinetics under the studied conditions. This is in contrast to Fig. 20, where the CO_2 capture rate decreases with increasing temperature and pressure when ATR is employed. The lower CO_2 capture rate at high temperatures may be attributed to the

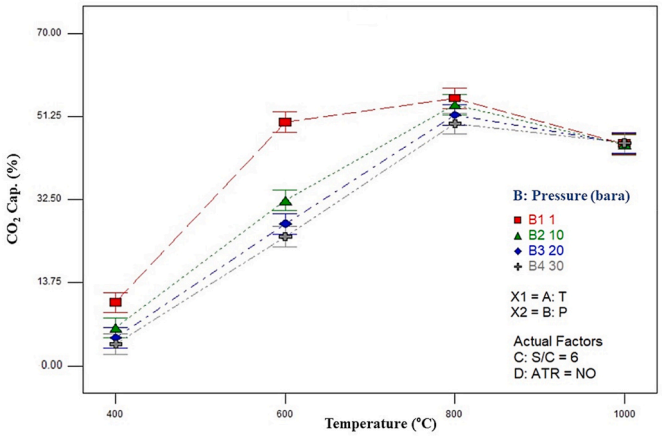

Fig. 19. Effect of temperature on CO_2 Capture for fixed S/C at 6 and at different pressure in the absence of ATR.

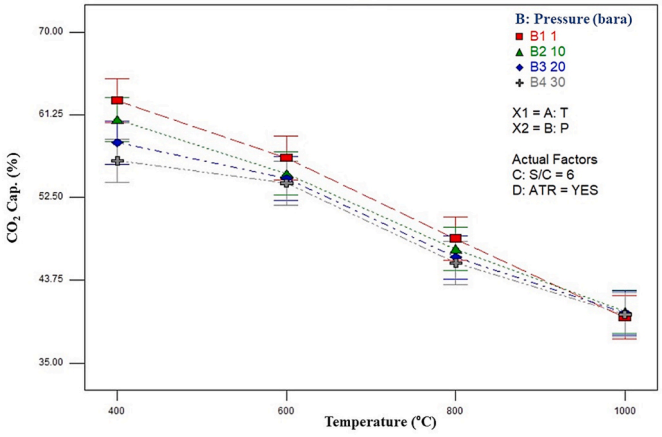

Fig. 20. Effect of temperature on CO_2 Capture for fixed S/C at 6 and at different pressure in the presence of ATR.

enhanced $CaCO_3$ decomposition at elevated temperatures. The crossing of the graphs in Fig. 20 at 1000 °C indicates that the effect of pressure on the CO_2 capture rate becomes negligible at this temperature. Comparing both graphs shows that utilising ATR helps to have a higher CO_2 capture rate at lower temperatures. The maximum CO_2 capture when ATR is absent is 54% at 800 °C, while the maximum CO_2 capture in the presence of ATR is 61% at 400 °C.

The results in Fig. 21 and Fig. 22 indicate that the CO_2 capture rate is not affected by the pressure in the range of 1–30 bara, regardless of the presence or absence of ATR. This suggests that the pressure has no significant effect on the carbonation process, which is consistent with previous studies on CO_2 sorption behaviour (Oakeson and Cutler, 1979). The parallel lines observed in the graphs for different S/C values indicate that there is no interaction between pressure and S/C in terms of CO_2 capture rate, which implies that the effect of S/C on CO_2 capture rate is independent of pressure.

In both graphs, the CO_2 capture rate increases with increasing S/C, indicating that higher steam-to-methane ratios lead to more efficient CO_2 capture. This can be attributed to the fact that higher steam-to-methane ratios favour the reforming reaction, which produces more CO_2 to be captured by the sorbent. The observed increase in CO_2 capture rate with increasing S/C is consistent with previous studies on SE-SMR (Wang et al., 2011; Zhu et al., 2015).

Moreover, the results show that the CO_2 capture rate is slightly higher in the presence of ATR, compared to the case where ATR is not utilised. This could be attributed to the fact that ATR increases the concentration gradient of CO_2 for adsorption, consequently increasing the driving force between the gas bulk and sorption active site. Greater driving force leads to higher efficiency for CO_2 capture. Dropping the CO_2 capture efficiency may cause carbon formations on the catalytic bed which is an important problem on the industrial scale. Therefore, the S/C should be maintained at a high ratio (i.e. more than 3) (Masoudi Soltani et al., 2021). It is worth mentioning that if a sufficiently high S/C ratio is given within the reactor for both cases, the carbon formation can be reduced and consequently, the CO_2 capture efficiency be improved, which is in conjunction with Annesini et al.'s research (Annesini et al., 2007).

Fig. 23 confirms the effect of temperature on the CO_2 capture rate in the absence of ATR. Also, it shows that there is an interaction between temperature and S/C on the capture performance. The influence of S/C on the CO_2 capture rate is larger at high temperatures rather than at low temperatures. However, when ATR is utilised (Fig. 24), the dependence of the CO_2 capture rate on temperature has decreased, but S/C still affects the capture rate. In the presence of ATR, S/C and temperature show no interaction as the trends suggest.

3.3. The DoE-optimised KPIs

The use of DoE can be highly effective in identifying the optimal combination of input variables that lead to desired KPIs. The objective of optimisation is to maximise the KPIs while maintaining high pressure for storage purposes. The model determines that when ATR is present, the

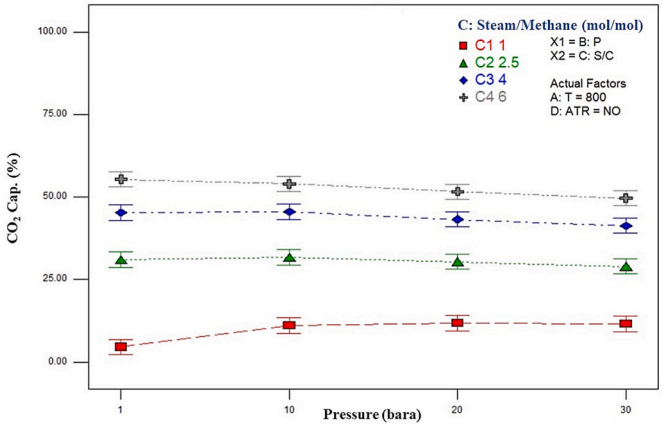

Fig. 21. Effect of pressure on CO_2 Capture at the fixed temperature of 800 °C and different S/C ratios in the absence of ATR.

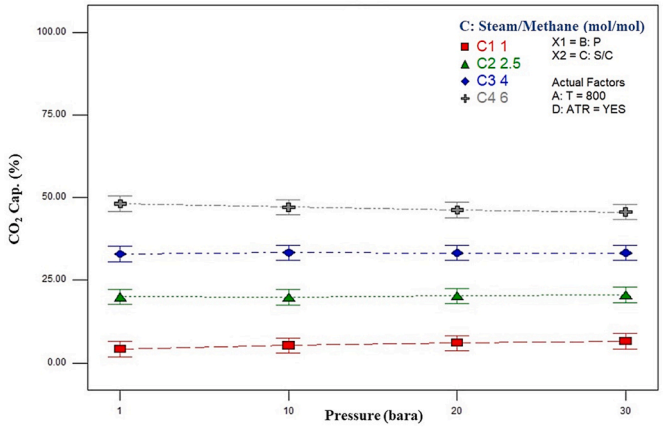

Fig. 22. Effect of pressure on CO_2 Capture at the fixed temperature of 800 °C and different S/C ratios in the presence of ATR.

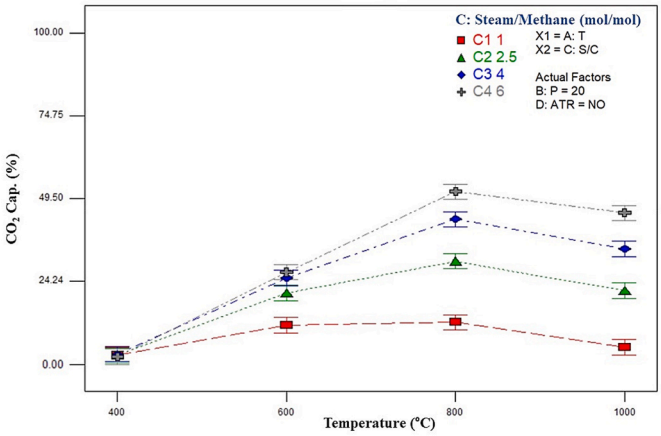

Fig. 23. Effect of temperature on CO_2 Capture at the fixed pressure at 20 bara and different S/C ratios in the absence of ATR.

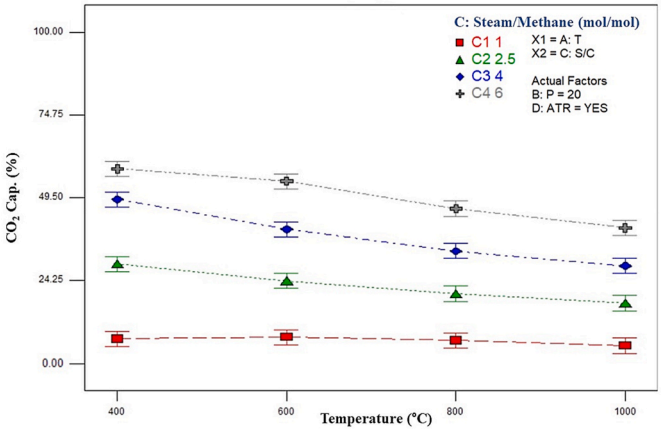

Fig. 24. Effect of temperature on CO_2 Capture at the fixed pressure at 20 bara and different S/C ratios in the presence of ATR.

highest KPIs (hydrogen purity = 86%, hydrogen yield = 36%, methane conversion = 99% and carbon capture rate = 50%) can be achieved at the temperature of 720 °C, the pressure of 20 bara, and the S/C ratio of 6.

However, if not using the ATR, the temperature, pressure, and S/C ratio should be 975 °C, 20 bara and 6, respectively. At this condition, the hydrogen purity is 84%, hydrogen yield is 42%, methane conversion is 96% and carbon capture rate is 48%.

A comprehensive comparison of the case with ATR and the case without ATR is illustrated in Fig. 25. It can be seen that when using ATR, the process's overall performance improves. Also, this improvement can be achieved at lower temperatures, which are more desirable on an industrial scale.

We can say that using ATR in SE-SMR leads to higher hydrogen purity of 86%, and a carbon capture rate of 50% while the hydrogen yield and methane conversion are still in the same range of the No-ATR case. The use of ATR also allows for these high KPIs to be achieved at lower temperatures, which can lead to cost savings by reducing the need for external heating, as the ATR reaction provides the necessary heat to drive the steam reforming reaction. This can result in lower capital and operating costs for the overall process.

To validate the DoE model, two simulations ran at the optimum parameters mentioned in Fig. 25, and the results and the Relative Standard Deviation (RSD) are listed in Table 5. Except for the hydrogen yield in the case of using the ATR unit, the other KPIs show an excellent agreement between the process simulation and the DoE model.

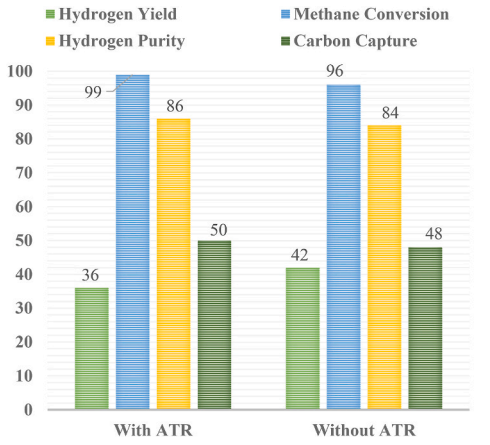

Temperature (°C)	720	975
Pressure (bara)	20	20
Steam-to-Methane ratio	6	6

Fig. 25. The optimum KPIs at different T, P and S/C for the case with methane combustion and the case without methane combustion.

Table 5
Validity of the DoE model based on the relative standard deviation (RSD%).

Scenario	Operating condition	KPIs (%)	Simulation	DoE Model	Relative Standard Deviation (RSD%)
With ATR Unit	720 (°C) 20 (bara) 6 (S/C)	H_2 Yield	37.13	36	3.04
		CH_4 Conversion	99.63	99	0.63
		H_2 Purity	86.92	86	1.05
		CO_2 Capture	52.02	50	3.88
Without ATR Unit	975 (°C) 20 (bara) 6 (S/C)	H_2 Yield	43.75	42	4.00
		CH_4 Conversion	96.60	96	0.62
		H_2 Purity	85.88	84	2.18
		CO_2 Capture	46.91	48	2.32

4. Conclusion

This study has developed a comprehensive kinetic model of the hydrogen production process with *in-situ* carbon capture for both SMR and the ATR processes. The developed one-dimensional heterogonous reactor model in Aspen Plus incorporated a kinetic-based model to define Steam Methane Reforming (SMR) and Water Gas Shift (WGS) reactions. The process model was subsequently optimised *via* the integration of DoE (General Full Factorial Design) for the optimisation of four pre-defined KPIs (H_2 yield, H_2 purity, CH_4 conversion, and CO_2 capture rate). The accuracy of the developed kinetic model was confirmed by comparing our simulation results to experimental data from the literature. The mean error of 3.19%, indicates a high degree of accuracy in our model's predictions. The key results are shown in the list below.

- Employment of ATR allows for an increased CO_2 capture rate (50%) at reduced temperatures (720 °C), showing a greater performance in comparison to SMR;
- Using ATR significantly impacts the methane conversion rate;
- There is an interaction between the S/C ratio and temperature which affects the methane conversion rate.

Finally, the application of DoE proved to be a highly effective method for determining the optimal combination of input variables that lead to the desired KPIs. The results of the optimisation showed that the presence of ATR improves the process's overall performance. This improvement can be achieved at lower temperatures, which are more desirable on an industrial scale and can lead to cost savings by reducing the need for external heating. Using ATR leads to higher hydrogen purity, methane conversion and carbon capture rate, while the hydrogen yield is still in the same range. The results obtained from the DoE model were validated by running simulations at the optimum parameters. The results showed excellent agreement between the process simulation and the DoE model. In summary, our study provides insight into the optimisation of operating parameters to maximise the KPIs in the clean hydrogen production process, considering the employment of ATR. Further research can be conducted to validate the findings and explore other operational variables and/or scenarios that were not considered in this study.

Credit author statement

Shervan Babamohammadi: Writing (Original Draft), Methodology, Software, Validation, Formal Analysis, Investigation, **William George Davies**: Writing (Review & Editing), Investigation, **Salman Masoudi Soltani**: Supervision, Funding Acquisition, Writing (Review & Editing), Resources, Conceptualisation, Project Administration.

Declaration of competing interest

The authors declare that they have no known competing financial interests or personal relationships that could have appeared to influence the work reported in this paper.

Data availability

Data will be made available on request.

Acknowledgements

This work has been funded by the UK's Engineering and Physical Sciences Research Council (EPSRC) under the project titled "Multi-physics and Multiscale Modelling for Safe and Feasible CO_2 Capture and Storage - EP/T033940/1". The authors are grateful to the Council for their support of this work.

References

Abbas, S.Z., Dupont, V., Mahmud, T., 2017a. Kinetics study and modelling of steam methane reforming process over a NiO/Al_2O_3 catalyst in an adiabatic packed bed reactor. Int. J. Hydrogen Energy 42 (5), 2889–2903. https://doi.org/10.1016/j.ijhydene.2016.11.093.

Abbas, S.Z., Dupont, V., Mahmud, T., 2017b. Modelling of H_2 production in a packed bed reactor via sorption enhanced steam methane reforming process. Int. J. Hydrogen Energy 42 (30), 18910–18921. https://doi.org/10.1016/j.ijhydene.2017.05.222.

Abbas, S.Z., Dupont, V., Mahmud, T., 2017c. Modelling of high purity H_2 production via sorption enhanced chemical looping steam reforming of methane in a packed bed reactor. Fuel 202, 271–286. https://doi.org/10.1016/j.fuel.2017.03.072.

Al-Malah, K., 2016. Aspen Plus®: chemical engineering applications. In: Aspen Plus®. Wiley Online Books.

Amini, Y., Hassanvand, A., Ghazanfari, V., Shadman, M.M., Heydari, M., Alborzi, Z.S., 2023. Optimization of liquid-liquid extraction of calcium with a serpentine microfluidic device. Int. Commun. Heat Mass Tran. 140, 106551 https://doi.org/10.1016/j.icheatmasstransfer.2022.106551.

Annesini, M.C., Piemonte, V., Turchetti, L., 2007. Carbon formation in the steam reforming process: a thermodynamic analysis based on the elemental composition. Paper presented at the Chem Eng Trans, ISCHIA Island Gulf of Naples, 24- 27 June.

Antzara, A., Heracleous, E., Bukur, D.B., Lemonidou, A.A., 2015. Thermodynamic analysis of hydrogen production via chemical looping steam methane reforming coupled with in situ CO_2 capture. Int. J. Greenh. Gas Control 32, 115–128. https://doi.org/10.1016/j.ijggc.2014.11.010.

Babamohammadi, S., Shamiri, A., Borhani, T.N., Shafeeyan, M.S., Aroua, M.K., Yusoff, R., 2018. Solubility of CO_2 in aqueous solutions of glycerol and monoethanolamine. J. Mol. Liq. 249, 40–52. https://doi.org/10.1016/j.molliq.2017.10.151.

Babamohammadi, S., Yusoff, R., Aroua, M.K., N Borhani, T., 2021. Mass transfer coefficients of carbon dioxide in aqueous blends of monoethanolamine and glycerol using wetted-wall column. J. Environ. Chem. Eng. 9 (6), 106618 https://doi.org/10.1016/j.jece.2021.106618.

BEIS, 2022. UK Hydrogen Strategy. Retrieved from Department for Business, Energy & Industrial Strategy. https://www.gov.uk/government/publications/uk-hydrogen-strategy.

Brown, M., Murugan, A., Foster, S., Heap, C., Pritchard, M., 2019. *Hydrogen Purity – Final Report* (10123173-Final Purity, Rev. 05). Retrieved from Department for Business, Energy & Industrial Strategy: https://www.hy4heat.info/s/WP2-Report-final.pdf.

Cherbański, R., Molga, E., 2018. Sorption-enhanced steam-methane reforming with simultaneous sequestration of CO_2 on fly ashes – proof of concept and simulations for gas-solid-solid trickle flow reactor. Chemical Engineering and Processing - Process Intensification 124, 37–49. https://doi.org/10.1016/j.cep.2017.11.010.

Crippa, M., Guizzardi, D., Banja, M., Solazzo, E., Muntean, M., Schaaf, E., Pagani, F., Monforti-Ferrario, F., Olivier, J., Quadrelli, R., Risquez Martin, A., Taghavi-Moharamli, P., Grassi, G., Rossi, S., Jacome Felix Oom, D., Branco, A., San-Miguel-Ayanz, J., Vignati, E., 2022. *CO_2 Emissions of All World Countries - 2022 Report*. Retrieved from Publications Office of the European Union, Luxembourg. https://doi.org/10.2760/07904.

Di Giuliano, A., Gallucci, K., 2018. Sorption enhanced steam methane reforming based on nickel and calcium looping: a review. Chemical Engineering and Processing - Process Intensification 130, 240–252. https://doi.org/10.1016/j.cep.2018.06.021.

Durakovic, B., 2018. Design of experiments application, concepts, examples: state of the art. Period. Eng. Nat. Sci. 5 (3), 421–439. http://pen.ius.edu.ba/index.php/pen/article/view/145.

El Hajj Chehade, A.M., Daher, E.A., Assaf, J.C., Riachi, B., Hamd, W., 2020. Simulation and optimization of hydrogen production by steam reforming of natural gas for refining and petrochemical demands in Lebanon. Int. J. Hydrogen Energy 45 (58), 33235–33247. https://doi.org/10.1016/j.ijhydene.2020.09.077.

Faheem, H.H., Tanveer, H.U., Abbas, S.Z., Maqbool, F., 2021. Comparative study of conventional steam-methane-reforming (SMR) and auto-thermal-reforming (ATR) with their hybrid sorption enhanced (SE-SMR & SE-ATR) and environmentally benign process models for the hydrogen production. Fuel 297, 120769. https://doi.org/10.1016/j.fuel.2021.120769.

Gorbounov, M., Petrovic, B., Ozmen, S., Clough, P., Masoudi Soltani, S., 2023. Activated carbon derived from Biomass combustion bottom ash as solid sorbent for CO_2 adsorption. Chem. Eng. Res. Des. 194, 325–343. https://doi.org/10.1016/j.cherd.2023.04.057.

Gorbounov, M., Taylor, J., Petrovic, B., Soltani, S.M., 2022. To DoE or not to DoE? A technical review on & roadmap for optimisation of carbonaceous adsorbents and adsorption processes. South Afr. J. Chem. Eng. 41, 111–128. https://doi.org/10.1016/j.sajce.2022.06.001.

Halabi, M.H., de Croon, M.H.J.M., van der Schaaf, J., Cobden, P.D., Schouten, J.C., 2008. Modeling and analysis of autothermal reforming of methane to hydrogen in a fixed bed reformer. Chem. Eng. J. 137 (3), 568–578. https://doi.org/10.1016/j.cej.2007.05.019.

IEA, 2021. Global Hydrogen Review 2021. IEA, Paris. Retrieved from. https://www.iea.org/reports/global-hydrogen-review-2021.

IPCC, 2022. Climate Change 2022: Mitigation of Climate Change. Contribution of Working Group III to the Sixth Assessment Report of the Intergovernmental Panel on Climate Change. https://doi.org/10.1017/9781009157926. Retrieved from.

Lee, D.K., Baek, I.H., Yoon, W.L., 2004. Modeling and simulation for the methane steam reforming enhanced by in situ CO_2 removal utilizing the CaO carbonation for H_2 production. Chem. Eng. Sci. 59 (4), 931–942. https://doi.org/10.1016/j.ces.2003.12.011.

Maqbool, F., Abbas, S.Z., Ramirez-Solis, S., Dupont, V., Mahmud, T., 2021. Modelling of one-dimensional heterogeneous catalytic steam methane reforming over various catalysts in an adiabatic packed bed reactor. Int. J. Hydrogen Energy 46 (7), 5112–5130. https://doi.org/10.1016/j.ijhydene.2020.11.071.

Masoudi Soltani, S., Lahiri, A., Bahzad, H., Clough, P., Gorbounov, M., Yan, Y., 2021. Sorption-enhanced steam methane reforming for combined CO_2 capture and hydrogen production: a state-of-the-art review. Carbon Capture Science & Technology 1, 100003. https://doi.org/10.1016/j.ccst.2021.100003.

Mehmeti, A., Angelis-Dimakis, A., Arampatzis, G., McPhail, S.J., Ulgiati, S., 2018. Life cycle assessment and water footprint of hydrogen production methods: from conventional to emerging technologies. Environments 5 (2), 24. https://doi.org/10.3390/environments5020024.

Meyer, J., Mastin, J., Bjørnebøle, T.-K., Ryberg, T., Eldrup, N., 2011. Techno-economical study of the zero emission gas power concept. Energy Proc. 4, 1949–1956. https://doi.org/10.1016/j.egypro.2011.02.075.

Mozaffarian, M., Soleimani, M., Bajgiran, M.A., 2019. A simple novel route for porous carbon production from waste tyre. Environ. Sci. Pollut. Control Ser. 26 (30), 31038–31054. https://doi.org/10.1007/s11356-019-06080-3.

NOAA, 2022. National Centers for Environmental Information, State of the Climate: Monthly Global Climate Report for Annual 2021 published online January 2022, retrieved on August 18, 2022 from. https://www.ncei.noaa.gov/access/monitoring/monthly-report/global/202113.

Oakeson, W.G., Cutler, I.B., 1979. Effect of CO_2 pressure on the reaction with CaO. J. Am. Ceram. Soc. 62 (11–12), 556–558. https://doi.org/10.1111/j.1151-2916.1979.tb12729.x.

Quirino, P.P.S., Amaral, A.F., Manenti, F., Pontes, K.V., 2022. Mapping and optimization of an industrial steam methane reformer by the design of experiments (DoE). Chem. Eng. Res. Des. 184, 349–365. https://doi.org/10.1016/j.cherd.2022.05.035.

Rodriguez, N., Alonso, M., Grasa, G., Abanades, J.C., 2008. Heat requirements in a calciner of $CaCO_3$ integrated in a CO_2 capture system using CaO. Chem. Eng. J. 138 (1), 148–154. https://doi.org/10.1016/j.cej.2007.06.005.

Saberimoghaddam, A., Nozari, A., 2017. An experimental and statistical model of a cyclic pressure swing adsorption column for hydrogen purification. Kor. J. Chem. Eng. 34 (3), 822–828. https://doi.org/10.1007/s11814-016-0314-0.

Shahid, M.M., Abbas, S.Z., Maqbool, F., Ramirez-Solis, S., Dupont, V., Mahmud, T., 2021. Modeling of sorption enhanced steam methane reforming in an adiabatic packed bed reactor using various CO_2 sorbents. J. Environ. Chem. Eng. 9 (5), 105863 https://doi.org/10.1016/j.jece.2021.105863.

Silva, J.M., Trujillano, R., Rives, V., Soria, M.A., Madeira, L.M., 2017. High temperature CO_2 sorption over modified hydrotalcites. Chem. Eng. J. 325, 25–34. https://doi.org/10.1016/j.cej.2017.05.032.

Singh, A.P., Singh, S., Ganguly, S., Patwardhan, A.V., 2014. Steam reforming of methane and methanol in simulated macro & micro-scale membrane reactors: selective separation of hydrogen for optimum conversion. J. Nat. Gas Sci. Eng. 18, 286–295. https://doi.org/10.1016/j.jngse.2014.03.008.

Wang, Y., Chao, Z., Chen, D., Jakobsen, H.A., 2011. SE-SMR process performance in CFB reactors: simulation of the CO_2 adsorption/desorption processes with CaO based sorbents. Int. J. Greenh. Gas Control 5 (3), 489–497. https://doi.org/10.1016/j.ijggc.2010.09.001.

Wang, Y., Memon, M.Z., Seelro, M.A., Fu, W., Gao, Y., Dong, Y., Ji, G., 2021. A review of CO_2 sorbents for promoting hydrogen production in the sorption-enhanced steam reforming process. Int. J. Hydrogen Energy 46 (45), 23358–23379. https://doi.org/10.1016/j.ijhydene.2021.01.206.

Xu, J., Froment, G.F., 1989. Methane steam reforming, methanation and water-gas shift: I. Intrinsic kinetics. AlChE J 35 (1), 88–96. https://doi.org/10.1002/aic.690350109.

Yan, Y., Thanganadar, D., Clough, P.T., Mukherjee, S., Patchigolla, K., Manovic, V., Anthony, E.J., 2020. Process simulations of blue hydrogen production by upgraded sorption enhanced steam methane reforming (SE-SMR) processes. Energy Convers. Manag. 222, 113144 https://doi.org/10.1016/j.enconman.2020.113144.

Zhu, L., Li, L., Fan, J., 2015. A modified process for overcoming the drawbacks of conventional steam methane reforming for hydrogen production: thermodynamic investigation. Chem. Eng. Res. Des. 104, 792–806. https://doi.org/10.1016/j.cherd.2015.10.022.